Philco-Ford Corporation
A Subsidiary of Ford Motor Company
Aeronutronic Division
Ford Road
Newport Beach, California

INTERIM REPORT

Effects of Impingement of Rocket Exhaust Gases and Solid Particles on a Spacecraft

PREPARED FOR: Jet Propulsion Laboratory
California Institute of Technology
Pasadena, California

UNDER CONTRACT: 951246

PERIOD COVERED: March 18, 1966 to October 25, 1966

DATE OF REPORT: November 22, 1966

PREPARED BY: C. H. Lewis, R. D. Hackett, and W. C. Kuby

APPROVED: P. M. Sutton
P. M. Sutton
Manager
Physics Laboratory

This work was performed for the Jet Propulsion Laboratory, California Institute of Technology, sponsored by the National Aeronautics and Space Administration under Contract NAS7-100.

CONTENTS

LIST OF FIGURES

NOMENCLATURE

D_p	diameter of particle
D_{32}	volume to area mean diameter
I	radiant intensity
I_o	incident radiant intensity
M	Mach number
P	gas pressure
q	heat transfer flux
R_i	radial distance of point of interest from nozzle centerline
R_e	nozzle exit radius
S_t	target material shear strength
T	temperature
u_p	particle velocity
u_g	gas velocity
v	impact velocity
V	volume of target material removed in an impact
V_o	volume of impacting particle
Z	distance measured from end of the normal shock region to the point of interest
α	component of impingement angle defined on page
β	component of impingement angle defined on page
γ	ratio of gas specific heats
δ	cant angle of nozzle with respect to the surface
ϵ	nozzle expansion ratio
θ	shock angle

NOMENCLATURE (continued)

ξ	true impingement angle
ρ_g	gas density
ρ_p	impacting particle bulk density
ρ_t	target material bulk density
ϕ	ratio of particle nozzle mass flow to gas mass flow

SECTION 1

INTRODUCTION

This interim report describes the major results of work performed under JPL Contract 951246 during the period 18 March 1966 - 25 October 1966. This contract has the general objective of determining the design restraints imposed upon a spacecraft by the impingement of gases and solid particles emanating from a solid propellant rocket.

The program was divided into two phases, one analytic and the other experimental. The analytic phase included a literature review of the important aspects of the problem and the development of analytic techniques to quantitatively describe the effects. Included in this effort were a review of gaseous impingement effects, the development of computational methods for predicting the high altitude rocket plume flow field for a gas particle flow, and a review of hypervelocity impact work.

The experimental phase was devoted to study of the impingement damage effects of micron sized particles such as are found in solid propellant rocket exhausts. A helium gas flow facility and a hydrogen-oxygen rocket motor were used to accelerate micron sized Al_2O_3 particles to velocities ranging from 4000 ft/sec to over 10,000 ft/sec. These high speed particles impinged on instrumented target samples. Effects such as material removal, particle heating, and variation of surface reflectance were studied.

The impact damage experiments are first described, followed by the current results of flow field computer program development and the review of gaseous plume impingement effects.

SECTION 2

IMPACTION DAMAGE STUDIES

2.1 GENERAL DESCRIPTION

The objective of these studies is to gain more information about the problem of surface damage due to particle cloud impaction, in particular, for the case of micron-sized Al_2O_3 particles such as emanate from a solid propellant rocket motor. Considerable work has been done to date on hypervelocity impact of metal particles upon metal surfaces. This work has been concerned exclusively with single particle impaction and has involved particle sizes of 1/32 inch to 1/8 inch in diameter. These current experiments are concerned with delineating the differences between these single particle impacts and cloud effects.

Much of the conventional hypervelocity impact data can be represented by the correlation of Sorensen[1], in which the volume of material removed per impact is given by

$$\frac{V}{V_o} = 0.12 \left(\frac{\rho_p}{\rho_t}\right)^{\frac{1}{2}} \left(\frac{\rho_p v^2}{S_t}\right)^{0.845} \qquad (1)$$

If the particle impaction process could be considered as the sum of a series of independent single impactions, then the above equation could be applied directly to each impaction and the resultant material removal summed over the number of impacting particles to give the total damage. The experiments in this study provide a test of this possibility and also provide data from which one can ascertain the functional dependence of material removal on particle size, particle impaction velocity, particle impaction mass flux, and target surface strength. The ultimate objective of this work is to develop a model which can be used to calculate damage to a surface due to the impingement of a solid propellant rocket exhaust containing Al_2O_3 particles.

2.2 EXPERIMENTAL MEASUREMENTS

The experimental program consisted of two sets of experiments. In one set, helium gas was used in a Mach 5 supersonic nozzle to accelerate the Al_2O_3 particles to mass average velocities between 4400 ft/sec and 5800 ft/sec. In the second set, the combustion products of a H_2-O_2 rocket motor were used to accelerate the particles to about 9000 ft/sec. The Al_2O_3 used in all of the experiments were from a single lot and had a number of peak of about 1.2 microns diameter and a mass mean of 5 microns diameter (Figure 1). A long slender nozzle with a length to exit diameter ratio of 18 was used to achieve maximum particle speed. The 1 inch diameter cylindrical specimens were made of either 1100-0 or 6016-T6 aluminum alloy and were aligned with axis parallel to the flow, exposing the flat face. The total surface regression of these specimens was measured and the temperature history of the specimen surface was recorded during each test. Surface reflectance was also measured before and after each test.

2.2.1 HELIUM TESTS

The Helium Flow Facility[2] was used to produce reproducible high velocity gas-particle flows into which were placed aluminum impaction samples. Prior to being mixed with the particles, the helium gas passes through a pebble bed heater, the temperature of which controls the velocity that the gas ultimately reaches at the nozzle exit. Velocities about 35% higher than that for room temperature helium are possible. During a test, the particle feed rate is measured directly, the gas stagnation pressure is measured in order to determine gas flow rate, and light transmission measurements are made at the nozzle entrance and exit to determine the particle mean velocity and spatial distribution. The samples are placed approximately 2 inches from the exit of the nozzle, which is within the Mach cone of the nozzle. The transmission measurement is made about half way between the sample and the nozzle exit.

Initial tests using 6061-T6 and 1100-0 aluminum produced very small material losses[3]. At these experimental conditions, Sorensen's[1] correlation equation indicated large target mass loss should have been expected. These results indicated the possibility of a significant

particle size scaling law. Consequently tests were conducted to more adequately document the two-phase flow velocity to better evaluate the validity of a scaling law. This was done by using transmission measurements at the nozzle entrance and exit to verify the particle mass mean velocity. In terms of the incident beam, I_o, the transmitted beam, I, can be expressed as[4]

$$I/I_o = \exp\left[-\frac{3\emptyset\rho_g u_g L}{\rho_p u_p D_{32}}\right] \qquad (2)$$

At the nozzle entrance, the assumption is made that the particle velocity is that of the gas and a value of D_{32}, the volume to area mean particle diameter, is computed from the measured transmission. Using this computed value of D_{32} and the computed values of the gas density and velocity, particle velocity can be obtained from the measured transmission at the nozzle exit. Figure 2 contains plots of the particle velocity at the exit plane of the test nozzle for the different experimental conditions obtained in this study. These velocities were calculated using the Aeronutronic particle lag computer program. The experimentally derived values for the mass mean velocity ($D_p \approx 5$ micron) agree well with the theoretical calculations.

Preliminary calculations had shown that the particle velocity loss through the shock layer in front of the specimen would be small. A short series of experiments was conducted to verify this in light of the greatly reduced target mass loss. Since the shock layer thickness is proportional to the specimen diameter, the specimen diameter was varied over a factor of four, holding all other conditions constant. The variation in target mass loss as shown in Figure 3, was relatively small and indicates that the particle velocity drop in the shock layer is, in fact, small. Some of the variation obtained can be explained by the increased heat transfer with reduced specimen diameter causing a reduction in surface strength.

The remaining helium gas-particle tests made in the period covered by this report had the objectives of determining the functional relationship of target mass loss with particle velocity and with surface strength as well as investigating the particle scaling effect. These results are shown in Figure 4. The target surface temperature was measured by

a thermocouple located .100 inches back of the surface. A transient heat transfer analysis indicated that the surface temperature was within 5% of the measured thermocouple temperature. The shear strength used in the calculations was based on this temperature (Figure 5) for shear strength data.

2.2.2 HYDROGEN-OXYGEN ROCKET TESTS

In order to obtain particle velocities higher than those available with the helium facility, the combustion products of a H_2-O_2 rocket engine were used to accelerate the Al_2O_3 particles through a nozzle that was geometrically similar to the one used in the helium tests. The Al_2O_3 particles are introduced into the combustion chamber by means of a water slurry. The chamber temperature is low enough so that the particles do not vaporize or melt, thus the particle size distribution in the nozzle flow is known. The target location was also the same as in the helium tests. Experimental verification of the particle velocities could not be made in these tests because a light transmission apparatus has not been provided in the hot firing test section. However, due to the geometric simularity of the two nozzles and the proven accuracy of the particle lag calculations for the helium nozzle, it can be assumed with confidence that the computed values of particle velocity are correct. (Figure 2)

6061-T6 and 1100-0 Aluminum alloys were used as target materials for these experiments. The two principal variables, other than material, were the total amount of impacting particles as controlled by run time, and the surface temperature of the sample as controlled by water cooling. The surface temperature was deduced from the temperature measured by a thermocouple placed below the surface. Below the thermocouple was a transverse passage for the flow of cooling water. The heat absorbed by the water was determined by measuring the water temperature rise and the flow rate. During the initial part of each test, the nozzle flow was free from any particles. Following Fay and Riddell[5] and Boison and Curtiss,[7] a gas phase convective heat flux was calculated which was used in conjunction with the specimen thermocouple to determine the surface temperature prior to the impaction of any particles. Both transient calculations and examination of the specimen temperature - time history indicate that

temperature distribution in the specimen reached a steady value during the gas heating period (about 2 seconds). This equilibrium surface temperature has been used to determine the surface strength used in plotting the data in Figure 4. During the period of particle flow, it was evident that additional heating occurred due to particle impaction. As yet, it has not been possible to determine the surface temperature rise during particle impaction because the temperature distribution has been of a transient nature throughout the duration of the particle impact portion of the runs. The data from these tests shown in Figure 4 show the effect of this increased heat transfer. Proportionally more damage occurs as the amount of impacting particles increases, indicating that the surface strength is decreasing as the surface temperature is rising.

2.3 DISCUSSION OF RESULTS

While the analysis of the impingement damage data collected to date is still of a preliminary nature, several positive statements can be made. For the helium data and the H_2-O_2 rocket data where the total amount of particles are small, the variation of damage with particle velocity does follow the functional form of Sorensen's correlation as shown in Figure 4. Also for these same data there appears to be little correlation between damage and the material type. From the helium data, verification of the particle lag calculations and the resultant nozzle design was obtained by the use of light transmission measurements of the flowing particle cloud. Based on the computed particle velocities and the surface strength based on temperature measurements, the experimentally obtained damage results were compared with Sorensen's correlation equation which is applicable to conventional hypervelocity impact tests. Figure 4 shows that the particle damage obtained from micron-sized Al_2O_3 particles is from 100 to 1000 times less than that due to an equivalent volume of large particles ($d_p \approx .125$ inch). These results show that particle heating can be significant and that part of the subsequent experiments should be designed so that the effect of the particle heating can be determined.

The apparent lack of correlation between damage and the different strength aluminum alloys at low temperatures has not been explained. The data does indicate that there is a significant particle size scaling factor. It is possible that the mechanical properties of projectile material may be more significant for the micron-sized particles used in this study than

for large particles studied previously.[1] This could be associated with the lack of sensitivity of material removed to surface strength for the cold target tests. Whether this effect persists at higher temperatures cannot be determined as yet because of the heat transfer variations due to the particles.

Surface reflectance was measured before and after tests for several specimens. In every case the normal reflectance after particle impaction was at least 50 times less than before; independent of the amount of particles involved. The apparatus used wasn't capable of measuring a greater variation. For all of these cases, the particle volume flux was 5×10^{-2} cm^3/in^2 sec or greater in order to obtain detectable material removal. Additional tests should be performed for the sole purpose of measuring surface reflectance degradation at lower particle impaction rates.

Certainly, in subsequent work, the problem of particle heating will be studied; the effect and nature of the significant surface strength for different classes of materials needs to be better understood; and the effect of angle of impact will be investigated.

SECTION 3

GASEOUS PLUME IMPINGEMENT EFFECTS

The objective of the following paragraphs is to present methods which can be used to evaluate the effects of gaseous rocket exhaust plume impingement. The emphasis is on the development of a hand-book type procedure for making engineering estimates of the pressure and heat transfer on a surface located within an exhaust plume. This discussion will be limited to highly underexpanded plumes and regions in which there are no plume shocks such as the lip shock.

Any calculation of plume impingement effects is dependent upon the determination of reasonable exhaust plume profiles. These profiles should define the following local properties within the plume: (1) flow direction, (2) flow velocity, (3) static temperature, (4) static pressure, (5) local gas specific heat, and (6) gas molecular weight. The exhaust plume computer program[8] can be used to determine all of these parameters at any location within the plume. The effects of the gas plume impingement in two phase flow impingement situations become small with respect to the solid particle effects as the distance from the nozzle is increased. Therefore, no attempt will be made to describe the impingement effects of the gaseous plume in the rarefied or non-continuum flow regime. For most practical applications, flow with a freestream Mach number at 12 or greater is outside the continuum regime. The plume computer program utilizes the method of characteristics, which requires the assumption of flow continuity. Although this program is capable of developing the exhaust plumes beyond flow Mach numbers of 12, its use in these regions is highly speculative. Calculations of the gas plume impingement pressure and heating may be made at large Mach numbers, but the accuracy diminishes rapidly. In most cases the computed heat transfer and pressure are conservatively high.

3.1 PLUME IMPINGEMENT (UPSTREAM PROPERTIES AND TRUE ANGLE)

Schlieren photographs of highly underexpanded plumes impinging on large flat surfaces indicate that the impingement shock waves tend to remain close to the surface (see References 9 and 10) when the nozzle exit plane is more than one nozzle diameter from the surface and parallel to or canted outward from the surface. Under these conditions the impinging flow Mach number is generally greater than 5 and the conditions of hypersonic flow are applicable. To simplify the calculation of the flow properties at the surface, it will be assumed that the shock layer is very thin and lies very close to the surface. It is further assumed that (1) the boundary layer growth and mass addition do not lift the shock layer off the surface and (2) reflected shocks emanating from the nozzle do not affect the plume flow. Thus, it is possible to obtain the gas properties impinging on the surface by direct superposition of the surface in question on the fully developed plume profile. Essentially, this means that the plume flow field is not turned, distorted, or otherwise affected by the object being impinged upon until the plume actually impacts the surface of the object. Thus, with a scale drawing, the undistorted plume properties and true impingement angle (the smallest angle between the streamline and a plane tangent to the surface at the point of impingement) can be found at the point of concern on the intersecting surface or object. By turning the flow through the true impingement angle the local surface static pressure, temperature, and Mach number can be computed.

Figure 6 illustrates the superposition of an exhaust plume profile on a flat surface. From this figure it is obvious that the centerline impinging flow properties and true impingement angle can be directly determined, and in many cases a calculation of the surface pressure and heating on the centerline is sufficient for engineering estimates of the magnitude of the problem. However, in actual design applications it is often necessary to estimate the off-centerline pressure or heating profile which involve more complex trigonometric considerations. The following few paragraphs are devoted to illustrating the solution of the true impingement angle for several plume-surface impingement situations commonly encountered in spacecraft application.

The exhaust plume must first be defined graphically such that the angle between the nozzle axis and the line tangent to the stream line at the point of impingement can be determined (see Figure 6). Figures 6 and 7 illustrate a common situation where a nozzle is fired above a flat surface which is parallel to the nozzle axis ($\delta = 0$) and displaced radially from the nozzle a distance (r). The true impingement angle (ξ) for any point on the flat surface can be computed using the following equations:

$$\xi = \sin^{-1}(\sin\alpha \sin\beta)$$

where: $\alpha \equiv$ angle between the nozzle axis and the tangent to the streamline at the impingement point.

$\beta \equiv$ angle between the projected plane containing the streamline and the line tangent to the surface at the point of impingement in a plane parallel to the R-H plane.

Figure 8 illustrates the more general situation of a canted nozzle ($\delta \neq 0$) firing over a flat plate.

$$\xi = \sin^{-1}(\cos\delta \sin\alpha \sin\beta - \sin\delta \cos\alpha)$$

where: $\delta \equiv$ cant angle of nozzle with respect to the surface.

One of the more difficult solutions is that for a situation similar to a roll moment producing rocket firing over the surface of a cylindrical spacecraft. Figure 9 illustrates the geometric variables required to determine the true streamline impingement angle. The solution of the true impingement angle (ξ) can be found by using the variables illustrated in Figure 9 in the following equations:

$$\mu_o = \sin^{-1}\frac{x + h}{a_o}$$

$$\theta_i = \sin^{-1}(R_q/R_i)$$

$$\xi = \sin^{-1}(\cos\mu_o \sin\alpha_i \sin\theta_i - \sin\mu_o \cos\alpha_i)$$

Probably the most common use of solid propellant motors on space booster systems has been posigrade and/or retrograde stage separation. In this application the motor fires axially over the cylindrical surface of the booster or spacecraft (see Figure 10). The solution of the true impingement angle is, of course, easier for the off-centerline cases if the axis of the nozzle is parallel to the axis of the cylinder. However, nozzles canted outward from the surface are more common. Solutions for both cases are presented below.

Zero degree cant angle ($\delta = 0$):

True impingement angle $\xi = \sin^{-1}(\sin\alpha_i, \sin\beta_i)$

where: $$\beta_i = \tan^{-1}\frac{R_i + (a_o + r)\sin\theta_i}{(a_o + r)\cos\theta_i}$$

$$\theta_i = \sin^{-1}\frac{R_i^2 + r(2a_o + r)}{2R_i(a_o + r)}$$

See Figure 10a for: R_i, P, a_o, α_i

Nozzle canted to surface ($\delta > 0$):

True impingement angle = $\xi = \sin^{-1}[\cos\eta_i \sin\alpha_i \sin\beta_i - \sin\eta_i \cos\alpha_i]$

where: $$\eta_i = \tan^{-1}[\cos(\theta_i - \beta_i)\tan\delta]$$

$$\theta_i = \sin^{-1}[\sqrt{b_i^2 - C_i} - b_i]$$

$$b_i = \frac{R_o}{R_i\tan\delta} \qquad \phi_i = \sin^{-1}[\sin\theta_i \sin\delta]$$

$$C_i = \frac{a_o^2 - (R_o\cos\delta)^2 - R_i^2}{(R_i \sin\delta)^2}$$

$$\beta_i = \tan^{-1}\left[\frac{R_i \cos^2\phi_i + R_o(\sin\phi_i \sin\delta - \sin\theta_i}{\cos\theta_i(R_i \sin\phi_i \sin\delta + R_o \cos^2\delta)}\right]$$

See Figure 10b for R_i, R_o, δ, α_i, a_o

As can be seen from the above, the calculation of the true impingement angle can become a lengthy process. It is, however, possible to limit the number of off-center calculations by first obtaining the center-line distribution of pressure or heat transfer and then making impingement profiles with only a few off-center calculations. Many cases will require calculation of only 4 or 5 specific points in one or two off-center plane intersections.

3.2 SURFACE PRESSURE

With the assumptions that the plume surface interaction shock and boundary layer are very thin, it is possible to estimate the pressure at the surface by simply turning the flow through the true impingement angle. The static pressure, Mach number, and specific heat ratio can be found at the point of impingement within the undisturbed plume. The true angle can be found as described in the previous paragraphs. The most accurate method for computing the static pressure in the flow after it has passed through the plume-surface interaction shock and turned parallel to the surface is somewhat debatable. There are three generally accepted methods available: (1) two-dimensional normal and oblique shock theory, (2) Newtonian impact theory, and (3) modified Newtonian impact theory. For a given case the resulting local surface pressure can vary as much as 30% depending on the method used. The most conservative solution is generally given by the two-dimensional, normal and oblique shock theory, while the lowest, and often unconservative, values of recovery pressure are given by the modified Newtonian method. Table 1 presents a comparison of the pressure rise calculated by the three methods for typical impingement conditions. The specific heat ratio was assumed constant at $\gamma = 1.25$. Note in this table that the pressure rise computed by the two-dimensional solution is surpassed by the Newtonian solutions only at very high angles of impingement.

A comparison of plume impingement pressure computed by the two-dimensional shock theory and the Newtonian theory is made with actual test results in Reference 11. The plume used for these calculations was constructed by a method of characteristics computer program using a constant specific heat ratio. It was found that the actual impingement pressure was more closely approximated by the two-dimensional theory in the region near the nozzle where the surface pressures are the highest. The Newtonian calculations provide a better fit to the data in very low pressure region several nozzle diameters downstream of the nozzle. It should be pointed out that the assumption of constant specific heat ratio (i.e., γ frozen at the nozzle exit plane) produces a plume with conservatively high local static pressure and temperature. If a variable γ plume were used (i.e., γ computed locally by the computer program as a function of local temperature),

the two-dimensional shock theory will give a better approximation to the actual impingement pressure at distances farther from the nozzle. With the use of variable γ in the construction of the undisturbed plume, it is likely that the Newtonian solutions will result in low predictions of the local impingement pressure throughout the plume impingement region.

Table 1

Comparison of Methods for Computing the Pressure Rise Across Normal and Oblique Shocks

Impingement Angle	Flow Mach #	Pressure Rise Ratio P_2/P_1 2-Dimensional Shock Method	Newtonian	Modified Newtonian
23°	15	503	441	418
23	10	237	201	191
23	5	7.5	5.84	5.44
50	10	897	746	707
90	10	1110	1260	1205

To minimize the potential of making low predictions of the local impingement pressures, only the two dimensional shock theory is recommended and presented here.

Computer programs are generally available for computing oblique shock tables for various specific heat ratios at various increments of impinging angles and Mach numbers. However, the standard oblique and normal shock relationships may be solved by hand if necessary. The following equations for pressure and temperature rise across an oblique shock, equations (3) and (4), can be solved using equation (5). Equation (5) describes the relationship between the flow deflection angle, θ, which is assumed equal to the true impingement angle, and the shock wave angle, β. This equation may be solved by fixing θ and M, and iterating on β until both sides of the equation are equal. The value of β must be between $\sin^{-1}(1/M)$ and $\pi/2$.

$$\frac{P_2}{P_1} = 1 + \frac{2\gamma}{\gamma + 1}(M_1^2 \sin^2\beta - 1) \qquad (3)$$

$$\frac{T_2}{T_1} = 1 + \frac{2(\gamma - 1)}{(\gamma + 1)^2} \frac{M_1^2 \sin\beta - 1}{M_1^2 \sin^2\beta} (\gamma M_1^2 \sin^2\beta + 1) \qquad (4)$$

$$\tan\theta = 2 \cot\beta \frac{M_1^2 \sin^2\beta - 1}{M_1^2(\gamma + \cos^2\beta) + 2} \tag{5}$$

Local velocity downstream of the oblique shock may be computed from equations (4), (6), (7);

$$M_2 = \left\{\frac{1 + (\frac{\gamma - 1}{2})M_1^2 \sin^2\beta}{[\sin^2(\beta - 0)][\gamma M_1^2 \sin^2\beta - \frac{\gamma - 1}{2}]}\right\}^{\frac{1}{2}} \tag{6}$$

$$V_2 = M_2 \sqrt{\gamma g R T_2} \tag{7}$$

The use of the above equations (3) through (7) requires the assumption that the gas is thermally and calorically perfect.

Figure 11 illustrates the relationship between θ, M_1, and β. It should be noted that for a given M_1 there is a maximum deflection angle (θ). This simply means that, if the flow must be deflected more than this maximum angle, an oblique shock is not sufficient and additional turning takes place in the shock layer flow. The pressure in this region is generally determined by normal shock relations. When the deflection angle is sufficiently large that the normal shock relations are to be applied, the local pressure and temperature rise across the normal shock may be computed using the following equations.

$$\frac{P_2}{P_1} = 1 + \frac{2\gamma}{\gamma + 1}(M_1^2 - 1) \tag{8}$$

$$\frac{T_2}{T_1} = 1 + \frac{2(\gamma - 1)}{(\gamma + 1)^2} \frac{\gamma M_1^2 + 1}{M_1^2}(M_1^2 - 1) \tag{9}$$

The use of these equations, of course, requires the assumption that the gas is thermally and calorically perfect.

With the information presented in the above paragraphs it is possible to estimate the local plume impingement pressure profiles on flat or cylindrical surfaces. The local static pressure on the impingement surface is computed using the following steps: (1) establish the undisturbed exhaust plume profile, (2) determine the local static plume properties (P_1, M_1, γ) at the radial and axial location (located with respect to the nozzle)

of the point of interest on the surface, (3) compute the true impingement angle, and (4) compute the local static pressure on the surface at the point of interest with the normal or oblique shock relations. Pressure profiles on the surface can be estimated by computing the static pressure on the line directly beneath the nozzle and at several individual locations off this line and combining the results graphically. Since the plume profile and the normal and oblique shock tables can be obtained with the use of computer programs, the most difficult part of the calculation becomes the solution of the true impingement angle. However, this presents a problem only for points on the surface which are not in a plane which is perpendicular to the surface and which contains the nozzle axis (i.e., the off-centerline points of interest).

Pressure profiles computed in the above manner may be used to estimate structural loading and true thrust vector of this motor. In addition, the pressure computed and the method used may be applied directly to estimating the heat transfer from the exhaust plume to the surface.

3.3 SURFACE HEATING

The primary objective of the above few paragraphs was to present a method for establishing the pressure profiles resulting from gas plume impingement on a surface. However, the methods for predicting the local temperature and velocity of the gas at the impingement surface was also presented above. This information can be used in estimating the surface heat transfer from the exhaust plume impingement.

Probably the best experimental data available on heat transfer from a real rocket plume impingement on a surface in a near space environment was obtained by North American Aviation for the Apollo program (see Reference 11). During these tests a liquid rocket motor (about 90 lb. thrust with Aerozine 50 and N_2O_4 as the propellant) was fired over a flat plate instrumented for pressure and heat transfer. Variables in these tests included nozzle exit area ratio, distance from the nozzle to the surface, and nozzle cant angle. Correlation of the heat transfer data was accomplished in Reference 11 by adding correlation constants to generally accepted methods for computing stagnation point and laminar flow flat plate.

convective heat transfer. It was found in Reference 11 that over the entire range of test variables the flow along the surface at the plate was laminar and in the continuum flow regime. The motor chamber pressure for these tests was nominally 100 psia. Since the range of test parameter (i.e., distance from the surface, nozzle area ratio, and motor cant angle) envelop most of the practical range for spacecraft application, and since solid rocket motors used in upper stage or spacecraft application will probably have more than 100 psia chamber pressure, it is reasonable to expect that the assumption of continuum flow will be valid. The assumption of laminar flow along the surface is probably also good since the density of the flow is low and there is a favorable pressure gradient in the vacuum application.

The calculation of the heat transfer profile over a large surface requires the use of two separate heat transfer relationships: (1) stagnation heating (used in the normal shock region) and (2) laminar flat plate heat transfer (used in the oblique shock region). The general form of the Kemp and Riddel empirical satellite re-entry heating equation (Reference 12) was used with an empirically determined constant to correlate the convective heat transfer in the normal shock region. Equation 10 is a simplification of the correlating equation presented in Reference 11.

$$q_N = \frac{55000\left(\frac{P_2}{RT_2}\right)^{\frac{1}{2}}}{\epsilon + \frac{3h}{4R_e}} \left(1 - \frac{T_2}{T_T}\right)^{1.625} \left(1 - \frac{T_W}{T_T}\right) \qquad (10)$$

where: q_N = convective heat transfer in the normal shock region (BTU/ft^{2}sec)

P_2 = local static pressure at the surface (lbF/ft^2)

R = gas constant (1544/molecular weight) (ftlbf/lb$_m$ ^oR)

T_2 = local static temperature at the surface (^oR)

ϵ = nozzle area ratio

h = distance of nozzle above the surface (inches)

R_e = nozzle radius (inches)

T_T = plume gas stagnation temperature (^oR)

T_W = surface temperature (^oR)

The above equation is applicable only in the normal shock region. It should be pointed out that the point of peak gaseous plume impingement heating has been found experimentally to coincide with the point of peak impingement pressure. Consequently, the location of the peak heating does not necessarily occur in the normal shock region. In fact, the peak impingement pressure, and heating generally occur in the oblique shock region.

The form of the Van Driest laminar flow equation (Reference 13) was modified with a correlating constant to approximate the heat transfer in the oblique shock region. A simplification of the equation originally disclosed in Reference 11 is presented below (equation 11).

$$q_o = 5.39\times10^{-9}(T_2)^{1.075}(M_2)^{2.39}(\gamma g)^{1.195}(R)^{.695}\left(\frac{P_2}{Z}\right)^{.5}\left[1 + \frac{5.88}{(M_2)^2}\left(1 - \frac{T_W}{T_2}\right)\right] \quad (11)$$

where: T_2 = local static pressure at the surface (^oR)

T_W = surface temperature (^oR)

M_2 = local static Mach number downstream of the oblique shock

γ = plume specific heat ratio

g = 32.2 (ft lb m/lg f sec^2)

R = gas constant (1544/gas molecular weight (ft lb f/lb m ^oR)

P_2 = local static pressure at the surface (lbf/ft^2)

Z = distance measured from end of the normal shock region to the point of interest (ft)

It should be noted that the above equation will give erroneous solutions if the distance from the normal shock region (Z) becomes small. As previously mentioned, the peak surface heating coincides with the peak surface pressure. If the point at which the peak pressure occurs is in the oblique shock region, then equation (11) is valid for locations downstream of that point. If, however, the point of peak pressure occurs in or near the normal shock region, then the maximum heating computed in the normal shock region should be used at (or extrapolated to) the point of peak pressure. Figure 12 illustrates the combination of the cold wall convective heat transfer rates from both the normal and oblique shock region for a typical centerline impingement heating case.

Surface heating profiles may be constructed in a manner similar to that described earlier for surface pressure profiles. The only

significant problem in obtaining off-center heat transfer rates is establishing the proper length to be used in equation (11) for the oblique shock region heat transfer. An approximation can be made by constructing on the surface pressure profile the line separating the normal and oblique shock regions, and drawing a line along the surface from the point of interest radially toward the nozzle. The distance along this line from the point of interest to the line separating the normal and oblique shock regions may be used to approximate the value of Z. Actual surface streamlines may be constructed from the true impingement angles; however, the additional calculations and plotting required are not commensurate with the additional accuracy gained.

With the information presented in the above paragraphs it is possible to estimate the local plume impingement convective heating profiles on flat or cylindrical surfaces. The calculation of the convective heat transfer requires 5 general steps: (1) establish the undisturbed plume profile, (2) determine the local static plume properties (P_V,T_1,M_1,γ) at the radial and axial locations (located with respect to the nozzle) at the point of interest on the surface, (3) compute the true impingement angle, (4) compute the local static properties (P_2,T_2,M_2) on the surface at the point of interest with the normal or oblique shock relations, (5) compute the local convective heating with the appropriate (normal shock or oblique shock region) convective heat transfer equation.

SECTION 4

PLUME FLOW FIELD CALCULATIONS

The particle trajectory computer program has been completed and checked out. The gas flow field program which has been previously described[8] is still being checked out under another N.A.S.A. contract. The program should be completed in total in the near future and at that time, a detailed program description, input test, and program card deck will be delivered to J.P.L.

REFERENCES

1. N. R. Sorensen, Proc. of Seventh Symposium on Hypervelocity Impact, Vol. VI, page 281 (1965).

2. W. C. Kuby, "Proposal for Effects of Impingement of Rocket Exhaust Gases and Solid Particles on a Spacecraft," Aeronutronic Proposal No. P-15244(U), submitted to J.P.L., Aug. 1965.

3. W. C. Kuby, Fifth Monthly Progress Letter, "Effects of Impingement of Rocket Exhaust Gases and Solid Particles on a Spacecraft," Aeronutronic Div., Philco-Ford Corp., J.P.L. Contract No. 951246, 2 Sept. 1966.

4. R. A. Dobbins, et.al., "Measurement of Mean Particle Sizes of Sprays from Diffractively Scattered Light," AIAA Journal, Vol. 1, No. 8, Page 1882, Aug. 1963.

5. Alcoa Aluminum Handbook, 1964.

6. J. A. Fay and F. R. Riddell, "Theory of Stagnation Point Heat Transfer in Dissociated Air," J. Aero. Sci., 25, 73-85, 1958.

7. J. C. Boison and H. A. Curtiss, "An Experimental Investigation of Blunt Body Stagnation Point Velocity Gradient," ARS Journal, Page 130, Feb. 1959.

8. C. H. Lewis, Sixth Monthly Progress Letter, "Effects of Impingement of Rocket Exhaust Gases and Solid Particles on a Spacecraft," Aeronutronic Div., Philco-Ford Corp., J.P.L. Contract No. 951246, 27 Sept. 1966.

9. R. C. Bauer and R. L. Schlumpf, "Experimental Investigation of Free Jet Impingement on a Flat Plate," AEDC, Report No. AEDC-TN-60-223, March 1961.

10. A. R. Vick and E. H. Andrews, Jr., "An Experimental Investigation of Highly Underexpanded Free Jets Impinging upon a Parallel Flat Plate," NASA Langley, unpublished as of Sept. 1963.

11. E. T. Piesik and M. L. Lofland, "High-Vacuum Plume Impingement Test Report," North American Aviation (S&ID) Accession No. 86086-64 August 1964.

12. N. H. Kemp and F. R. Riddell, "Heat Transfer to Satellite Vehicles Re-entering the Atmosphere," Jet Propulsion, Vol. 27 (Feb. 1957).

13. E. R. Van Driest, Investigation of Laminar Boundary Layer in Compressible Fluids Using the Crocco Method, NACA TN 2597 (1952).

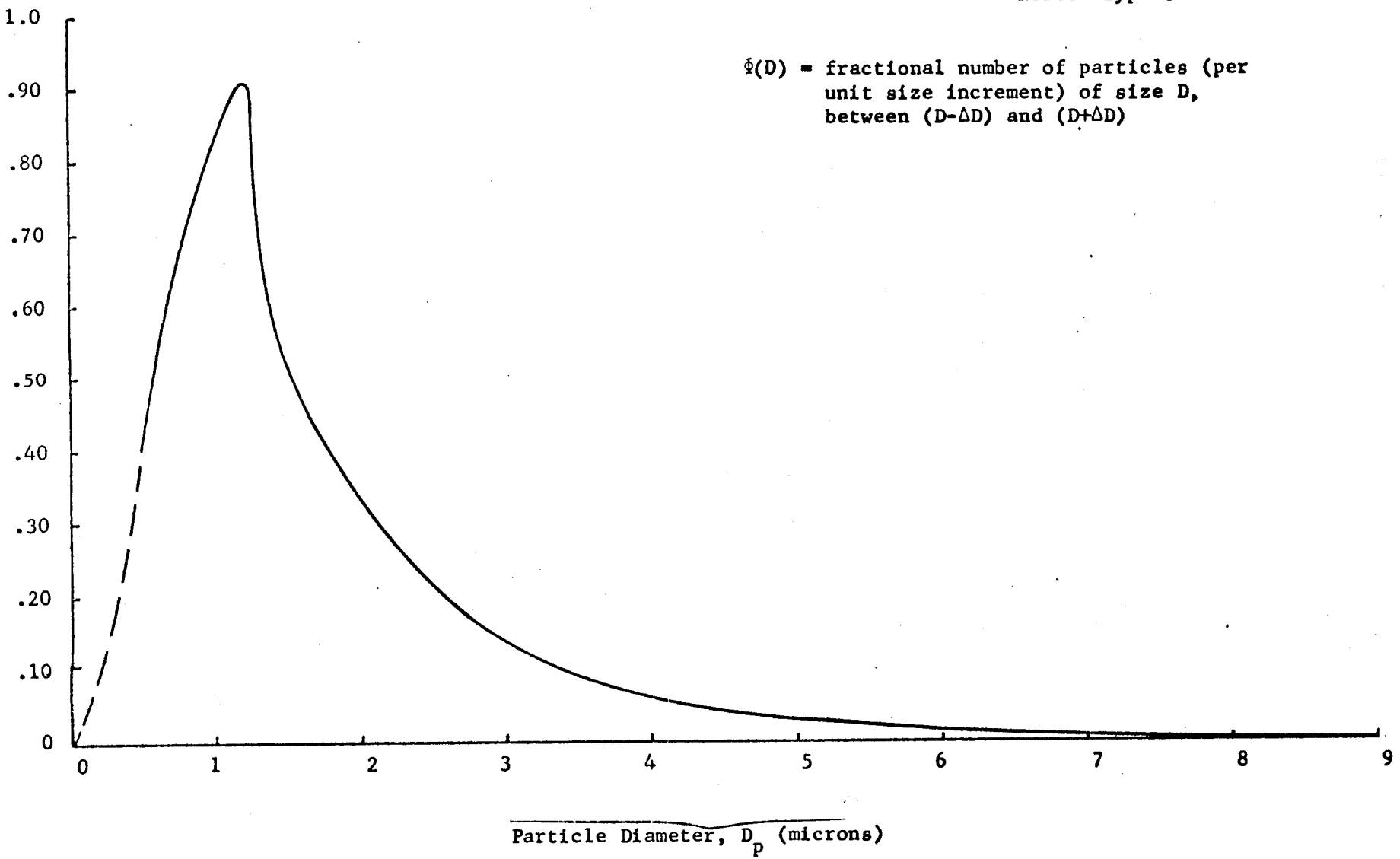

FIGURE 1 - PARTICLE SIZE DISTRIBUTION

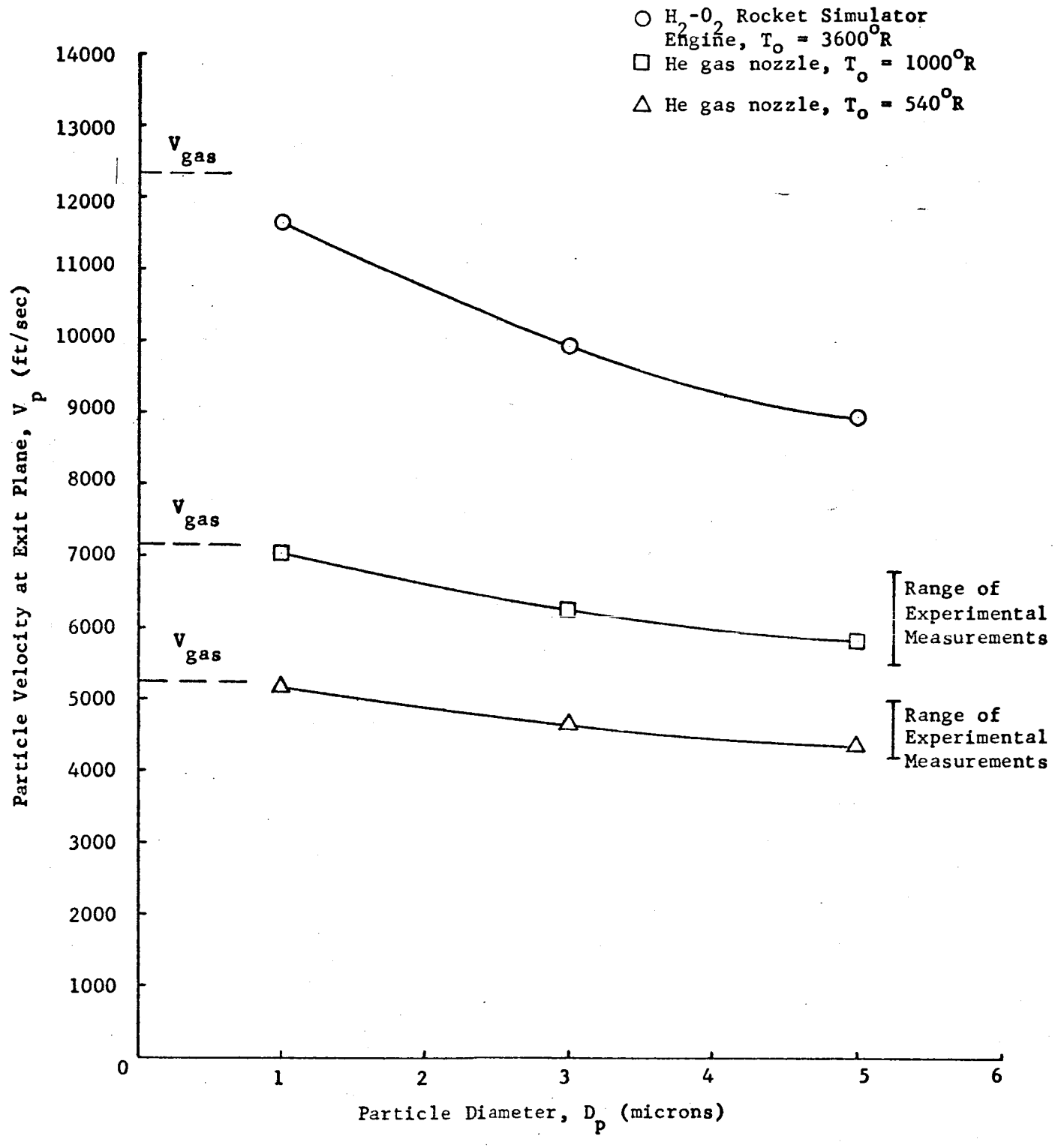

FIGURE 2 - Al_2O_3 PARTICLE VELOCITY AT NOZZLE EXIT PLANE

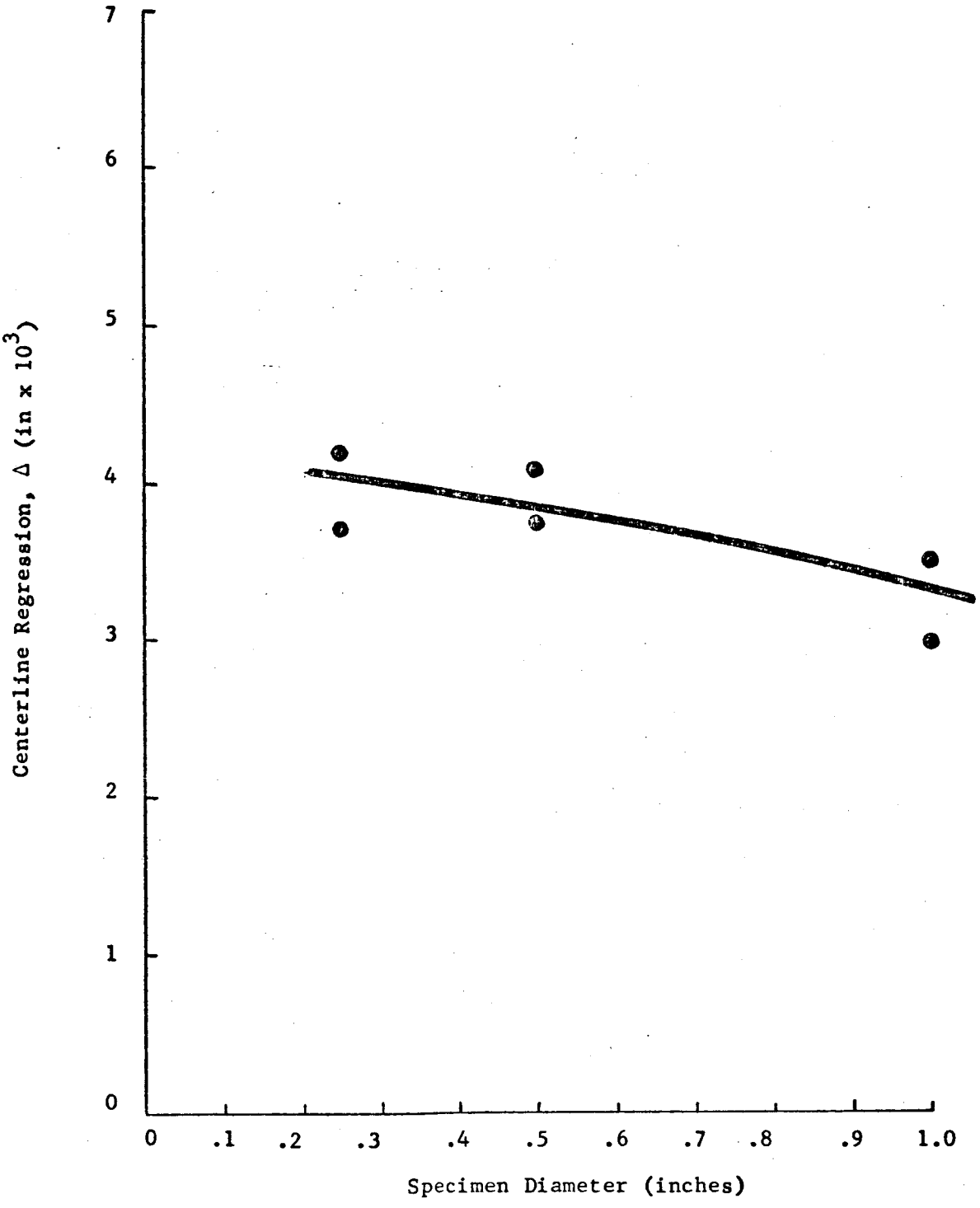

FIGURE 3 - IMPINGEMENT DAMAGE AS A FUNCTION OF SPECIMEN DIAMETER

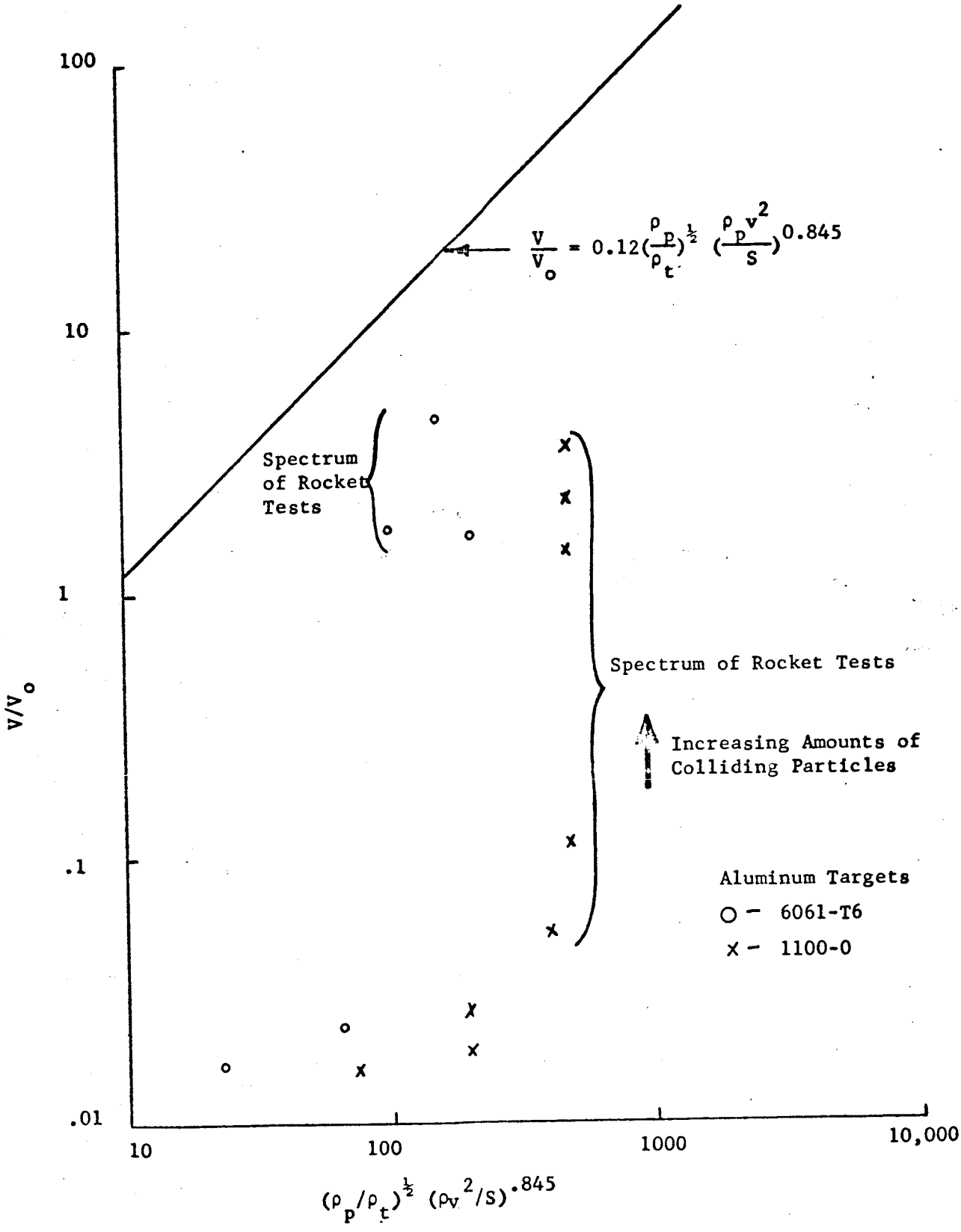

FIGURE 4 - NORMALIZED VOLUME LOSS FOR Al_2O_3 TO ALUMINUM IMPACTS

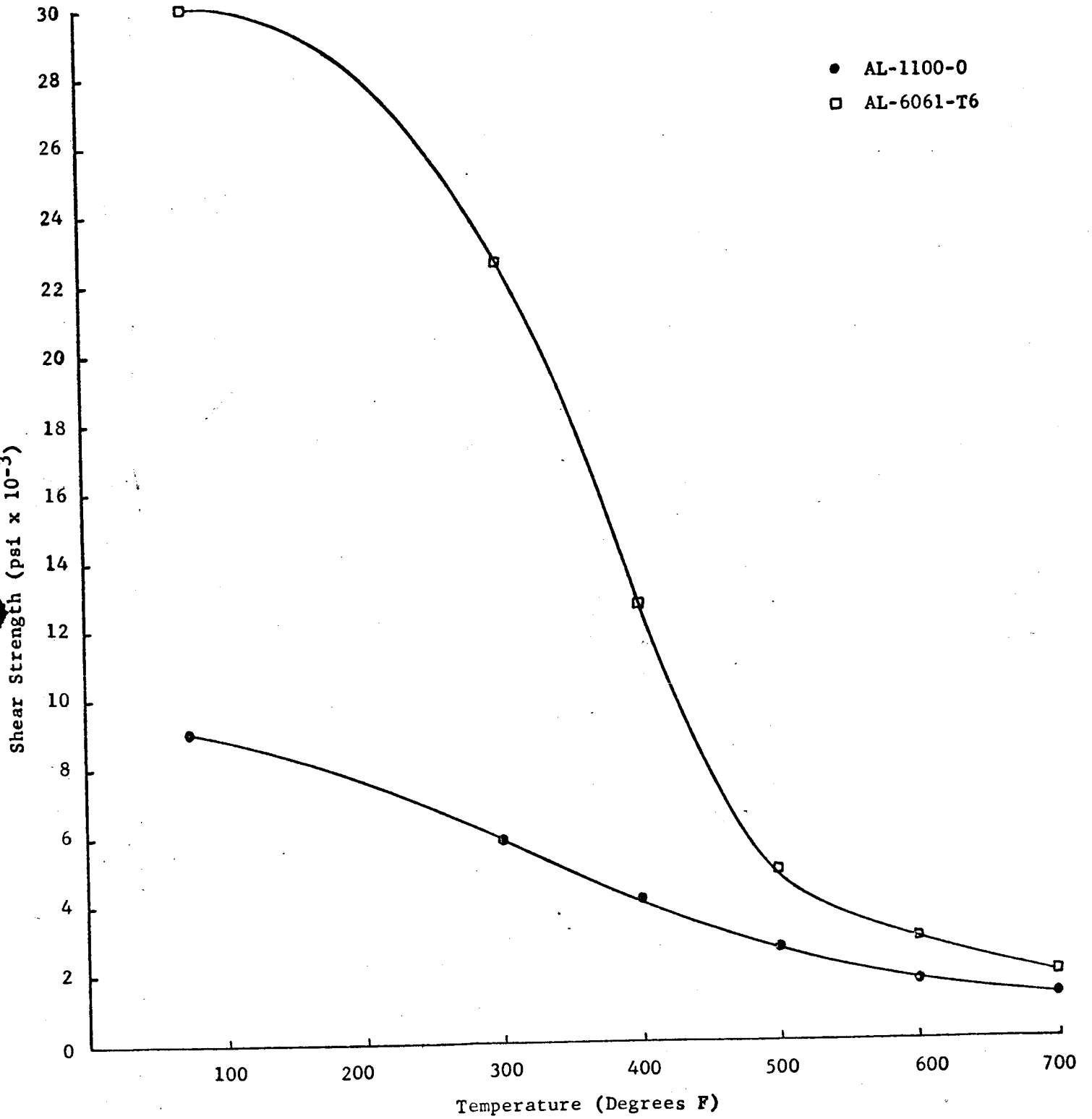

FIGURE 5 - SHEAR STRENGTH OF 6061 and 1100 ALUMINUM ALLOYS

UNCANTED NOZZLE FIRING OVER A FLAT SURFACE

— — — Lines of Constant Local Flow Properties P,M,T,γ

——— Flow Streamlines

——— Location of Centerline Impingement

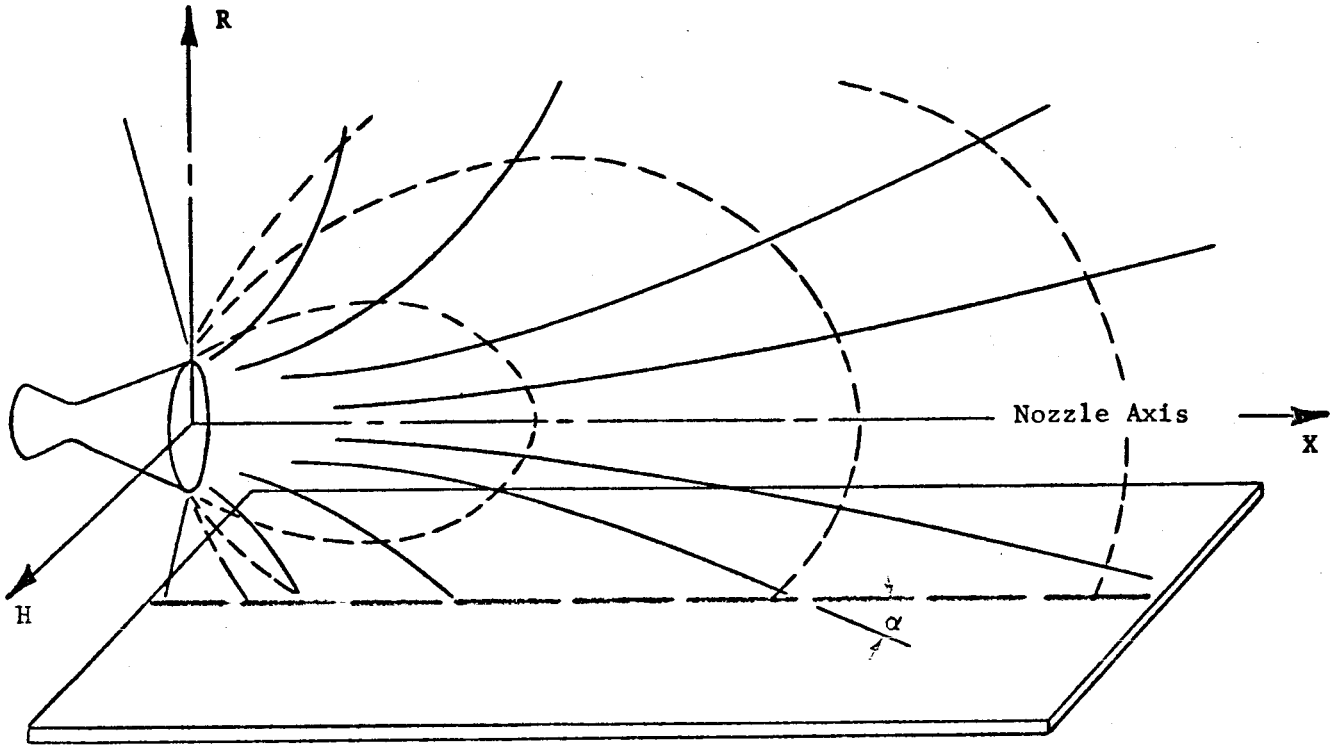

- α = True Impingement Angle for Centerline Case
- Impingement Surface Drawn Parallel to Nozzle Axis but Perpendicular to the Plane of the Plume (R-X)
- The Line on the Surface Called the Centerline is Defined by the Locus of Points Contained by Both the Plane of the Plume (which also Contains the Nozzle Axis) and a Plane which is Tangent to the Surface and Perpendicular to the Plane of the Plume

FIGURE 6 - ROCKET PLUME IMPINGEMENT ON A FLAT SURFACE (CENTERLINE CASE)

TRUE IMPINGEMENT ANGLE FOR UNCANTED NOZZLE
FIRING OVER A FLAT PLATE

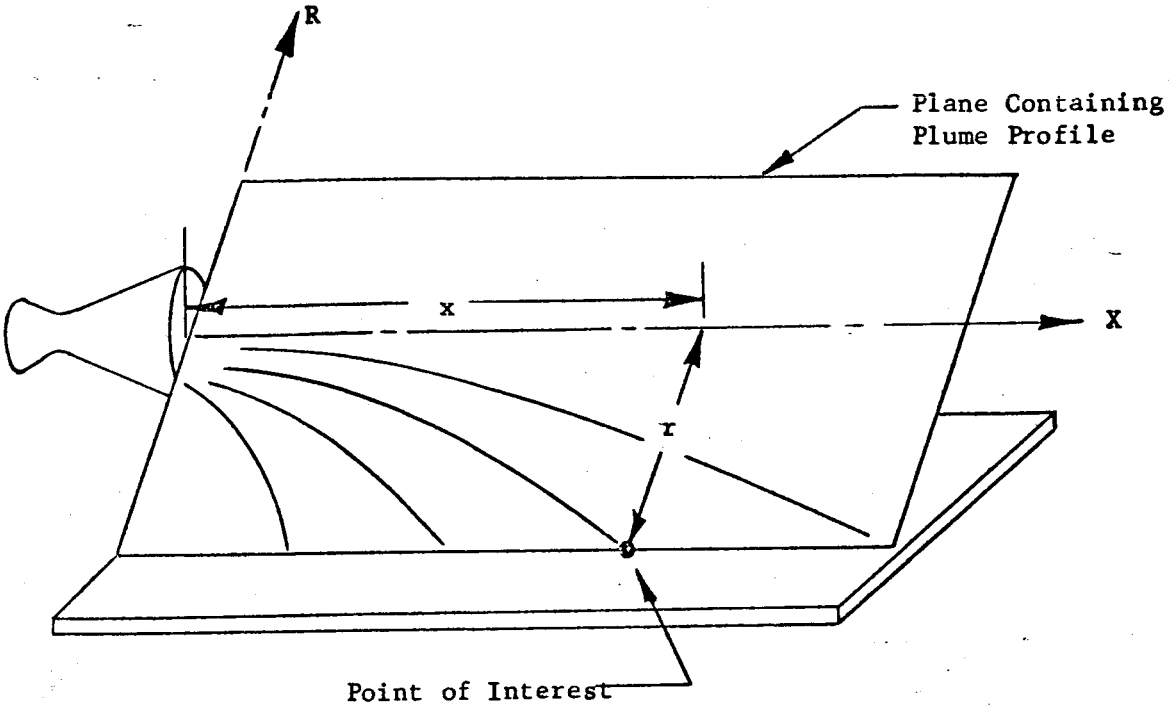

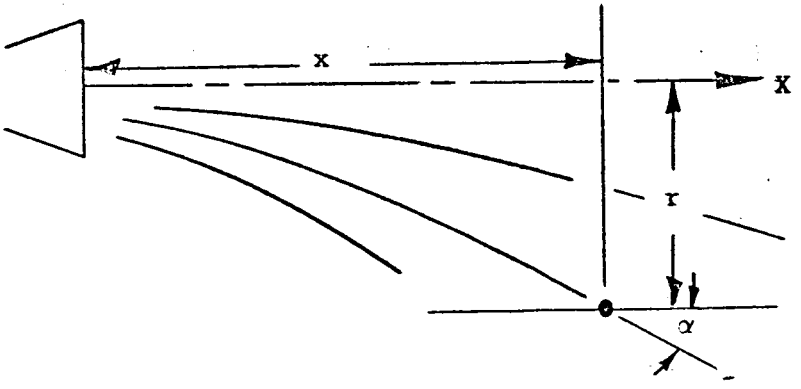

Plane View of Plume Profile

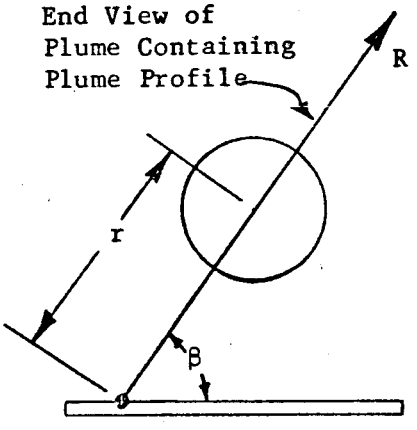

End View of Nozzle

FIGURE 7 - ROCKET PLUME IMPINGEMENT ON A
FLAT SURFACE (OFF CENTER CASE)

OFF CENTER IMPINGEMENT

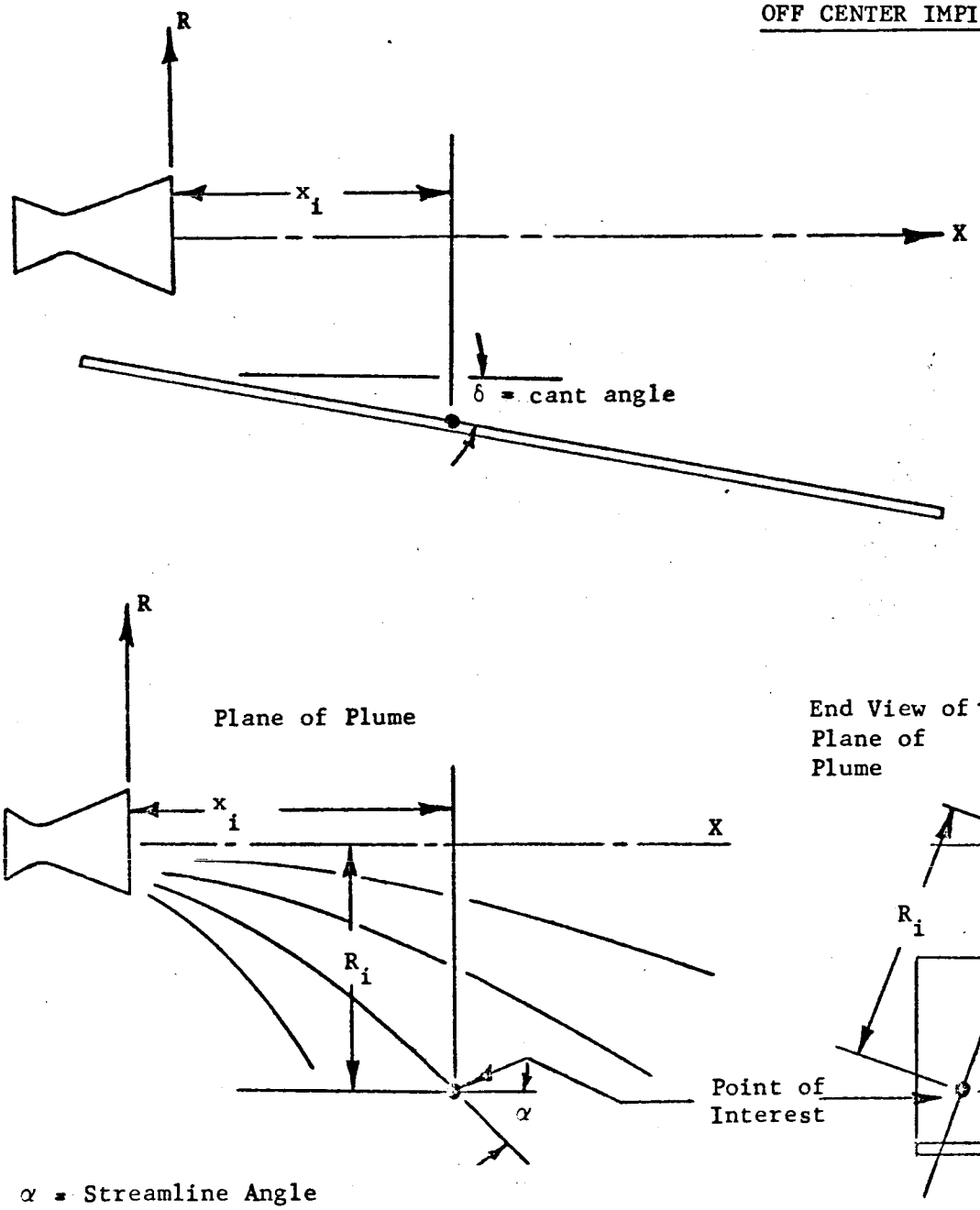

α = Streamline Angle
Measured with Respect
to Nozzle Axis -- not
the Canted Surface

FIGURE 8 - ROCKET PLUME IMPINGEMENT
ON A FLAT SURFACE

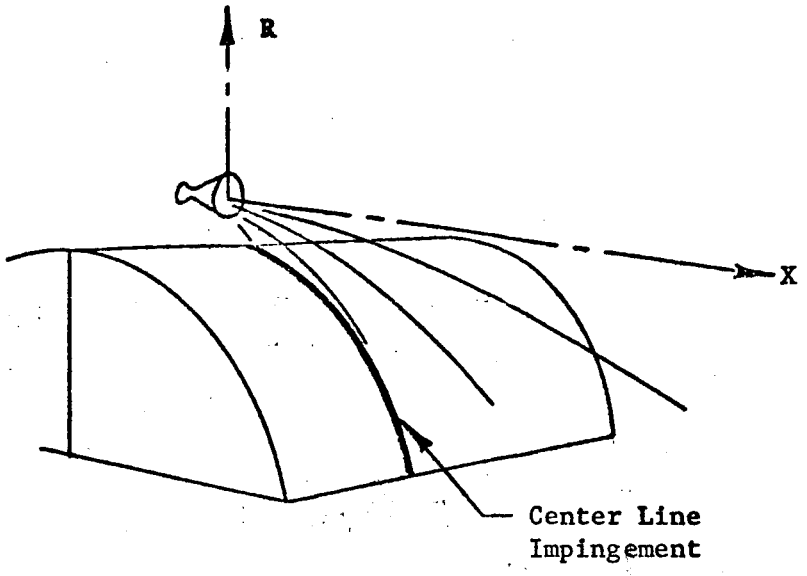

CENTER LINE IMPINGEMENT

- Plume Shown in R-X Plane
- R-X Plane Perpendicular to Cylinder Axis
- Impingement Properties and True Impingement Angle Read Directly

OFF CENTER IMPINGEMENT

- All Dimensions Normalized on the Nozzle Exit Radius
- α_o - Angle Between the Streamline and the Nozzle Axis at the Point of Interest

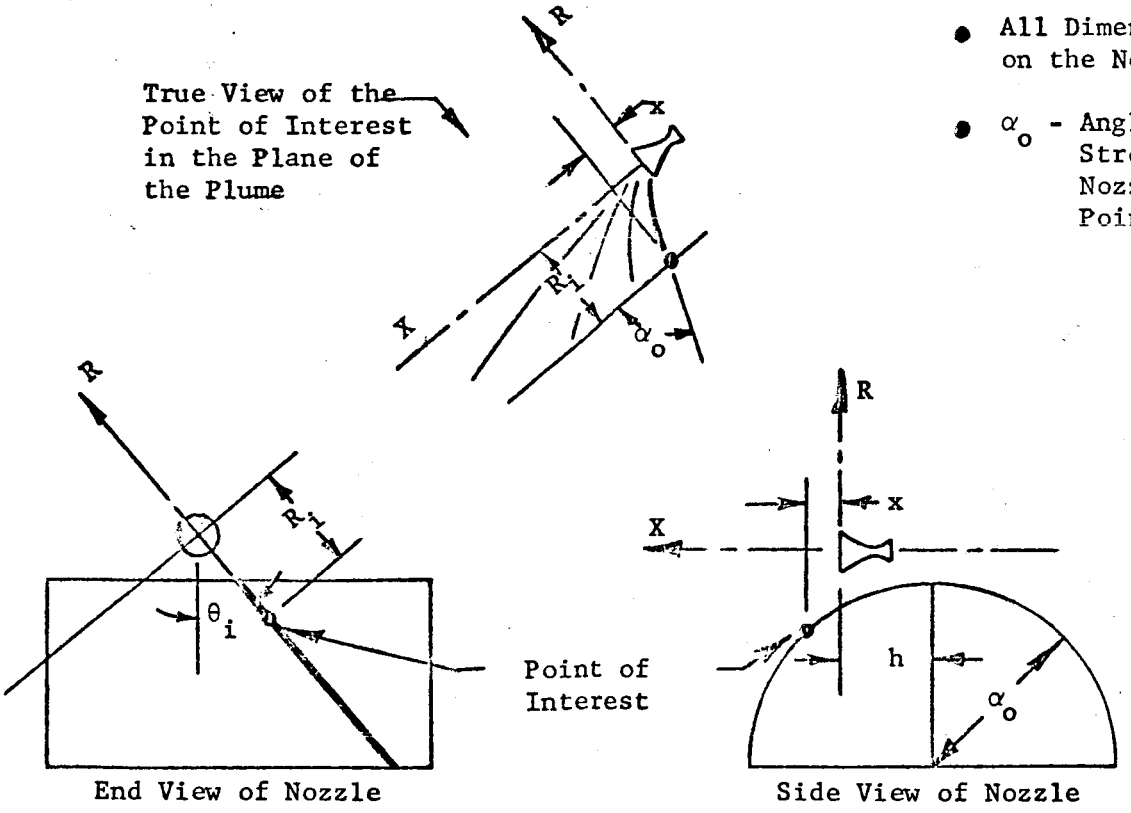

FIGURE 9 - ROLL ROCKET PLUME IMPINGEMENT ON A CYLINDRICAL SURFACE

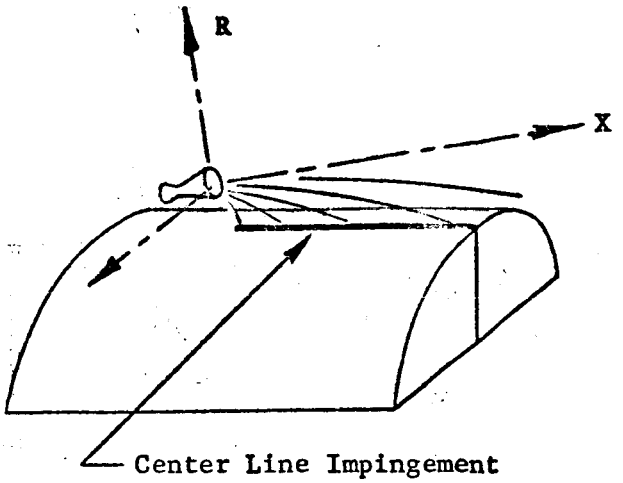

CENTER LINE IMPINGEMENT

- Plane of Plume Contains Axis of Cylinder
- Nozzle Axis (X) may be Parallel to or Canted to Cylinder Axis ($\delta \geq 0$)
- Impingement Properties and True Impingement Angle Read Directly

---

OFF CENTER IMPINGMENT
Uncanted Nozzle ($\delta = 0$)

- α_o = Angle Measured Between the Nozzle Axis and Streamline at the Point of Interest
- All Dimensions Normalized By Nozzle Exit Radius

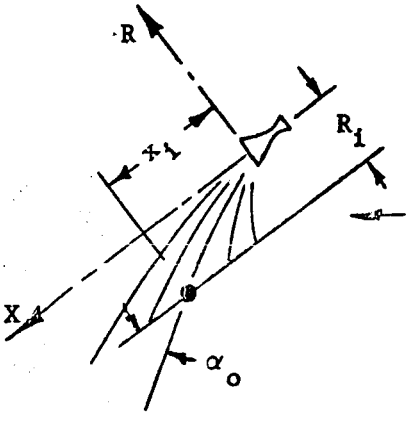

True View of the Plane Containing the Plume, Nozzle Axis, and the Point of Interest On the Cylindrical Surface

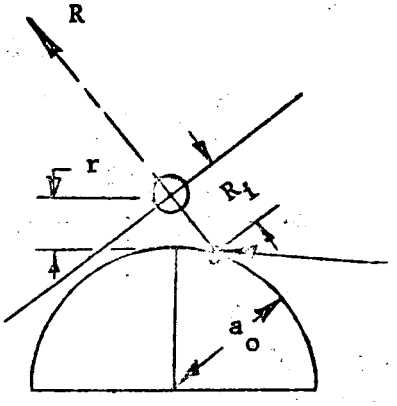

End View of Nozzle

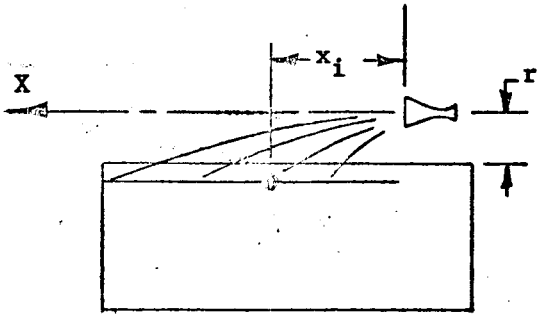

Side View of Nozzle

FIGURE 10a - PITCH OR YAW ROCKET PLUME IMPINGEMENT ON A CYLINDRICAL SURFACE

Off Center Impingement

(Canted Nozzle $\delta > 0$)

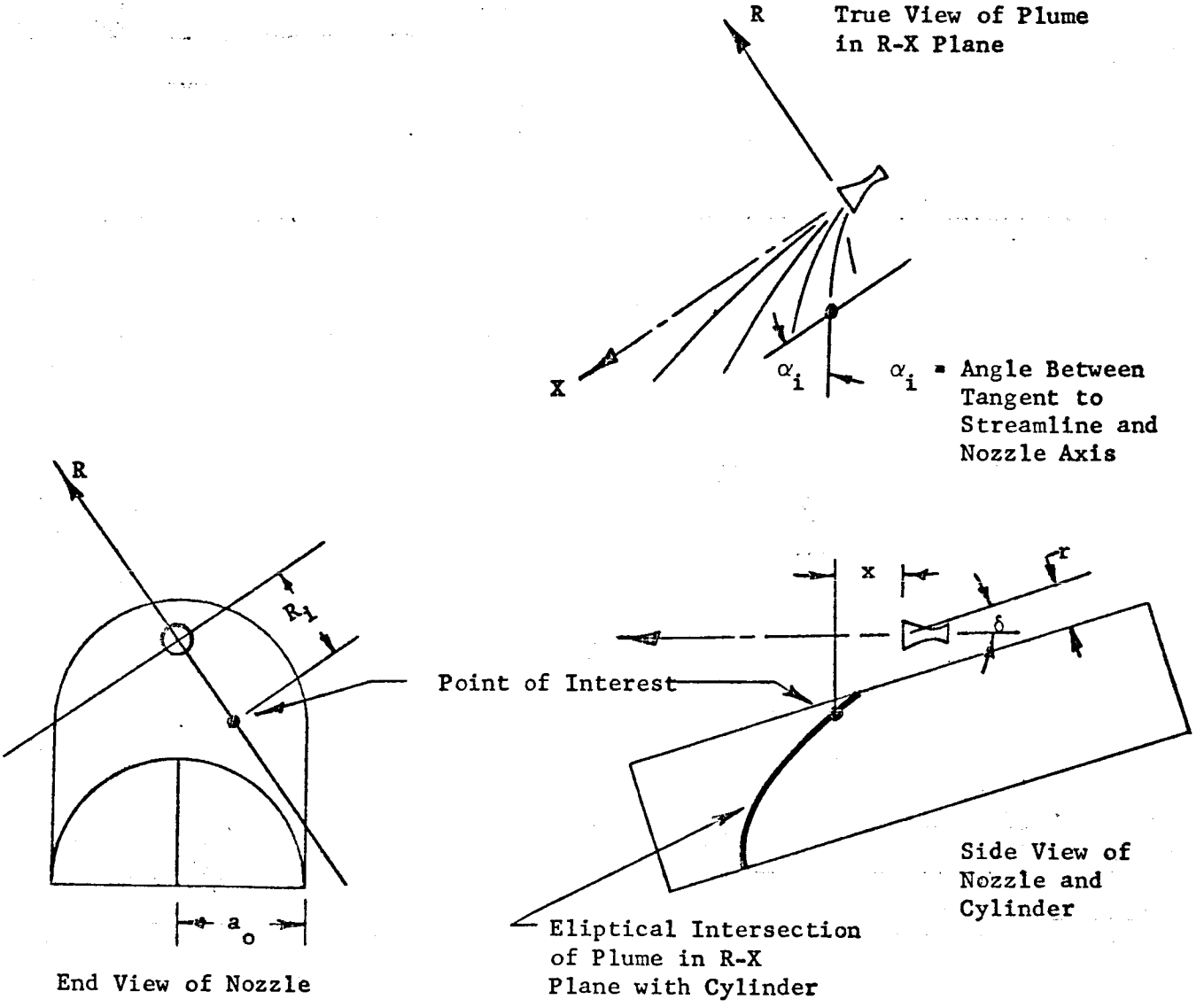

FIGURE 10b - PITCH OR YAW ROCKET PLUME IMPINGEMENT ON A CYLINDRICAL SURFACE

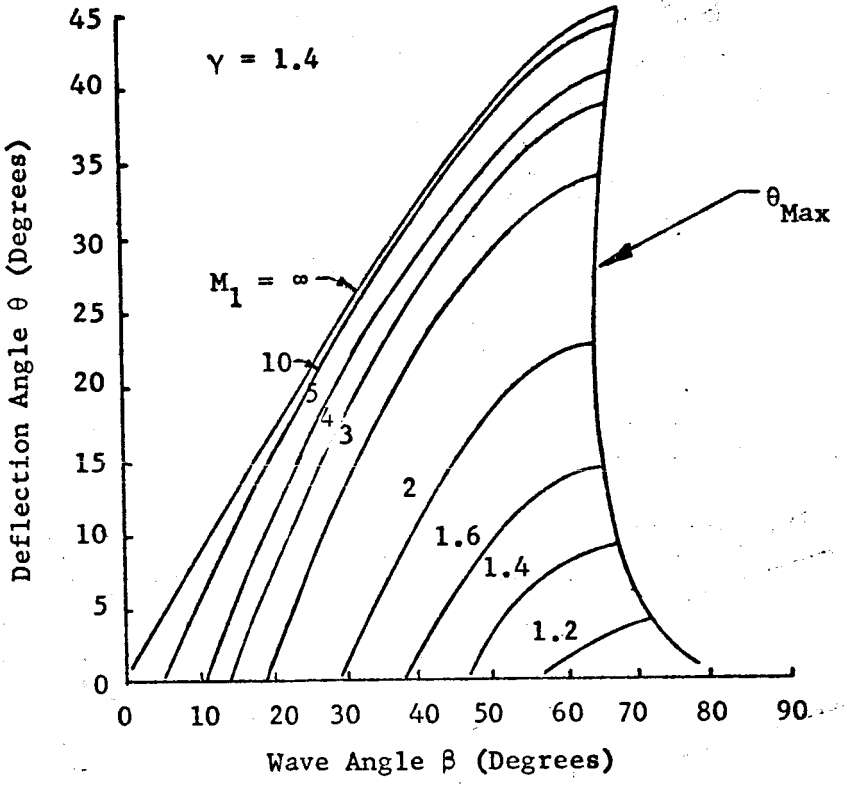

FIGURE 11 - OBLIQUE SHOCK SOLUTIONS

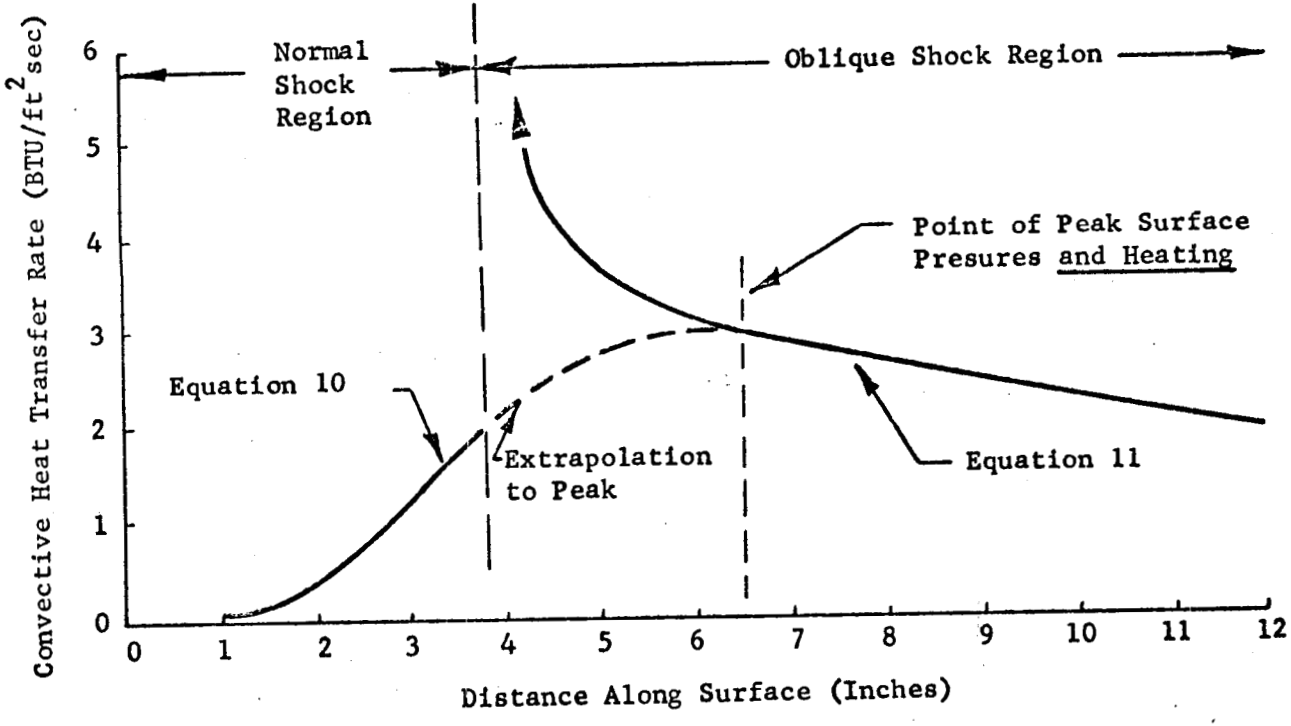

FIGURE 12 - TYPICAL CONVECTIVE HEAT TRANSFER DISTRIBUTION